
Conference or Workshop Item:
Lassila, T., Lange, M., Porras, A.R. et al. (2016) Electrophysiology Model for a Human Heart with Ischemic Scar and Realistic Purkinje Network. In: STACOM 2015, 9 October 2015, MICCAI 2015, Munich, Germany.

https://doi.org/10.1007/978-3-319-28712-6_10

Electrophysiology Model for a Human Heart with Ischemic Scar and Realistic Purkinje Network

Toni Lassila[1], Matthias Lange[1], Antonio R. Porras[2], Karim Lekadir[2], Xènia Albà[2], Gemma Piella[2], Alejandro F. Frangi[1]

[1] Centre for Computational Imaging and Simulation Technologies in Biomedicine (CISTIB), Department of Electronic and Electrical Engineering, The University of Sheffield, Sheffield, UK

[2] Centre for Computational Imaging and Simulation Technologies in Biomedicine (CISTIB), Department of Information and Communications Technologies, Universitat Pompeu Fabra, Barcelona, Spain

Abstract. We present a Purkinje-myocardium electrophysiology model that includes the scar plus a detailed Purkinje network, and compare simulated activation times to those obtained by electro-anatomical mapping in vivo. The results illustrate the importance of using sufficiently dense Purkinje networks in patient-specific studies.

1 Introduction

Personalised computational electrophysiology (EP) models are increasingly improving in the level of anatomical and physiological detail, and their personalisation, so as to hold the promise of enabling personalised planning of ablation targets in terminating ventricular tachycardias (VT). There is some evidence that certain type of arrhythmias may be triggered by ectopy arising from Purkinje fibers during acute myocardial infarction [2]. Until recently, however, most EP simulations have neglected the effect of the Purkinje network (PN) or used very coarse networks. Thus the first step towards more complete modelling of ventricular tachycardia (VT) is to develop realistic models of coupled myocardium-Purkinje whole-heart models, and to validate them against physiological measurements of activation patterns.

We present a computational pipeline for human EP modelling with: (i) a PN model based on a rule-based algorithm for generating the network and a set of cable equations on line segments coupled together by the gap junction resistance model [16]; (ii) a myocardium model based on the monodomain approximation and the left ventricular (LV) action potential (AP) model of Bueno-Orovio et al. [3]; and (iii) electrical remodelling in the scar/borderzone by fitting the model of Bueno-Orovio et al. to a modified ten Tusscher-Panfilov 2006 -model [14].

We then compare the model predictions against electro-anatomical mapping (EAM) data consisting of endocardial activation times in a patient with extensive myocardial scarring. The EAM data is projected onto the simulated LV geometry

to compare the local activation times (LAT). Results are given for varying levels of Purkinje-muscle junction (PMJ) density.

2 Models for Cardiac Electrophysiology

A standard monodomain approximation for myocardial tissue is used:

$$\chi \left[c_m \frac{\partial u}{\partial t} + i_{ion}, (u, v, r, s) - i_{app}(t) \right] = \nabla \cdot (\sigma \nabla u) \,, \tag{1}$$

where the ionic current, $i_{ion} = i_{\text{fi}} + i_{\text{si}} + i_{\text{so}}$, consists of the fast/slow inward, and slow outward currents respectively, which are gated by the internal membrane variables v, r, s as in Bueno-Orovio et al. 2008 [3]. The conductivity tensor in (1) depends on a spatially varying parameter γ s.t. $\sigma = (1 - \gamma_i) \left[\sigma_t I + (\sigma_l - \sigma_t) f_0 \otimes f_0 \right]$. To account for structural remodelling under chronic myocardial infarction, the conduction velocity (CV) in the deep scar and its surrounding border zone are typically modified. As first approximation the membrane model is turned off and the CV is set to zero throughout the deep scar region. However, experimental evidence on rabbits [17] indicates greatly reduced conductivity (10% of normal CV) in the borderzone surrounding the scar, but close to normal conductivity in the infarcted region (50% of normal CV), and in some cases even the possibility to stimulate the infarcted region. Accordingly, we used $\gamma_{\text{healthy}} = 0$, $\gamma_{\text{border}} = 0.97$, and $\gamma_{\text{scar}} = 0.75$, and the longitudinal and transversal conductivities are $\sigma_l = 1.5$ kOhm^{-1}cm^{-1}, $\sigma_t = 0.6$ kOhm^{-1}cm^{-1}. This corresponds to reducing the conduction velocity to 8% in the borderzone and 44% in the scar region. Fibre dispersion is not considered.

The effects of ischemia include hyperkalemia, changes in the fast Na^+ and L-type Ca^{2+} channels, hypoxia, and acidosis. These effects can be modelled in the ten Tusscher-Panfilov 2006 -model by adding an extra ATP-sensitive K^+ current, as was done in [6]. The extracellular potassium concentrations are kept at their normal levels to avoid elevated resting potentials. The modified parameters describing mild and severe ischemia are taken from [8].

Once the ten Tusscher-Panfilov 2006 -model has been extended, APs from rest are extracted. A subset of 7 parameters in the Bueno-Orovio et al. -model is selected for optimisation. A curve-fitting problem for the AP is solved and parameters that do not change from their reference values are replaced by educated choice. The process is repeated until an accurate replication of the AP shape is obtained. The final values of the modified parameters are (borderzone/scar): $k_w = 65.0356/65.0356$, $\tau_{o1} = 6.3196/5.3307$, $\tau_{so1} = 56.6591/56.1802$, $\tau_{so2} = 1.0809/1.5291$, $k_{so} = 2.2695/2.4552$, $\tau_{s2} = 7.3099/7.6184$, $k_s = 5.6456/5.7472$.

The PN is modelled as a network of line segments (with loops) with the model of Vigmond *et al.* [16]. We use the Di Francesco-Noble [4] membrane model with standard parameters for the PN. The conductivity and membrane model of the PN remains unchanged in the borderzone and scar regions. The numerical algorithm used for the PN is described in more detail in [7]. The connection between the PN and the myocardium is modelled using a coupled

resistor and distributed current source -model that captures the 3-5 ms delay in orthodromic propagation. We do not consider the antidromic conduction back into the PN in this work.

3 Computational Electrophysiology Model Generation

LV segmentation is performed from cardiac MRI with delayed enhancement (DE-MRI) as described in [12]. The segmentation thresholds have been previously optimized using EAM data in [1, 5]. These thresholds have been used to successfully identify borderzone conducting channels during catheter ablation. After projecting the intensity values to a surface mesh segmentation of the LV, 4,000 radial basis function interpolation sites are randomly seeded on the endo- and epicardial surfaces respectively. The intensity values are interpolated using inverse multi-quadric shape functions and used to choose the appropriate membrane model parameters using the same criterion as in [5] that intensity above >60% of maximum is considered scar, while <40% of the maximum is considered healthy tissue – everything in between is considered borderzone.

Rule-based Poisson interpolation is applied to obtain fibre orientations. The LV centreline is identified automatically and a linearly graded fibre orientation from -41° on the endocardium to $+60^\circ$ on the epicardium is obtained. Three levels of PNs of increasing density (166 PMJs in the low-density case, 756 PMJs in the mid-density case, and 1,296 PMJs in the high-density case) are generated to test the impact of PMJ density on the activation pattern. A 2 cm area below the basal cut-plane contains no PMJs as reported in literature. The resulting PN is fitted to the endocardium, but is not modified according to the LAT observed in the EAM. While methods exist [10, 11, 15] to fit the PMJ distribution to patient-specific observations of endocardial LAT, the danger of over-fitting the model to available data exists. Increasing the number of PMJs allows fitting of the LAT with arbitrary accuracy at least in the regions where the PN is present, but without necessarily providing meaningful information about the actual morphology of the PN. A crude fitting algorithm may, for example, prefer to eliminate the PN completely from the infarct scar region in order to match the LAT, which is not supported by the evidence of the PN surviving in the infarct core with prolonged action-potential duration and enhanced automaticity [9]. We therefore rely on the observations of [15] that even without personalising the PMJ locations, sufficiently dense tentative PNs can predict LAT with reasonable accuracy.

4 Results

The EAM dataset was obtained with the CARTO system (Biosense Webster, Haifa, Israel) and consisted of bipolar/unipolar voltages, LAT, and position of each catheter point on or near the endocardium. Measurements were made with a tetrapolar diagnostic catheter (Thermocool, Navistar, Biosense Webster) in a total of 671 locations on the LV endocardium and around the mitral annulus.

After having the segmentation from DE-MR, this was imported into CARTO and registration was done manually using the CARTO software during the intervention. The experimental methodology is described in more detail in [12]. The LV had considerable post-infarction myocardial scarring several days after the initial infarct (see Fig. 1). Previous studies [5, 13] have shown a moderate correlation between the scar regions obtained from EAM by bipolar voltage thresholds (<0.5 mV for the scar and 0.5–1.5 mV for the borderzone) and the DE-MRI-derived endocardial scar regions, so that we took treated the DE-MRI-derived scar regions as having been previously validated. Simulations were run for both the cases where the scar region was assumed to be nonexcitable tissue (not shown) and excitable tissue with the parameters identified by the nonlinear fitting procedure. While the subject's LV was heavily scarred both transmurally and apex-to-base on the lateral side, the EAM did confirm slow CV but not propagation failure in the scar regions. Thus the case of nonexcitable scar tissue was rejected due to insufficient activation of the LV scar region compared to the EAM results.

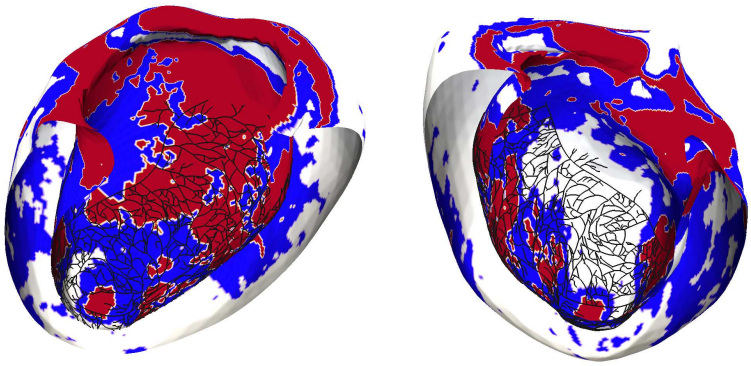

Anterior view Posterior view

Fig. 1. Scar and its borderzone identified from DE-MRI according to the criteria in [5]. Color scheme indicates red for deep scar, blue for borderzone, and white for healthy myocardium. Tentative PN superimposed for reference. Large percentage of PMJs in the posterolateral free-wall lie in the deep scar region.

Fig. 2 shows the LAT measured from EAM and interpolated onto the lateral endocardium (left) compared with the simulated LAT (right). Despite no personalisation being performed on the myofibre orientation nor on the PN, correspondence is good at the apex and mid-wall. The largest difference in LAT takes place near the basal regions. Fig. 3 shows the bullseye plot of mean LAT on each of the 17 AHA segments for the three different densities of PNs. As coverage improves, the LAT more closely corresponds to timings measured by EAM. The largest differences can again be observed at the basal area, which we explain as follows. In the EAM data there are some catheter locations that are

clustered near the aortic valve and the mitral annulus. Projecting the data from these points onto the truncated LV surface may produce spurious data that make the recorded basal LAT unreliable. We do not consider this a serious problem, as the basolateral region is known to activate last and therefore plays a lesser role in the induction of VT.

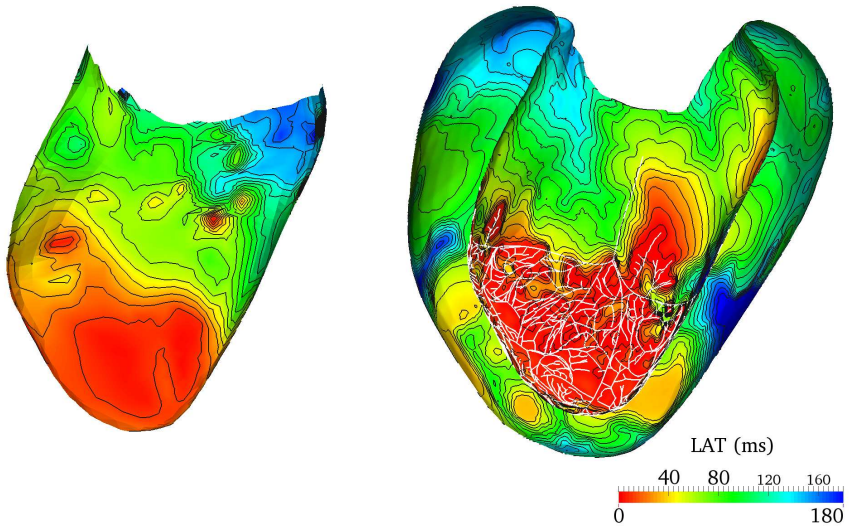

Electro-anatomical mapping Simulated activation

Fig. 2. The LAT on the septal endocardium for EAM (left) and simulation (right). Isochrones of LAT present every 10 ms. High-density PN superimposed on the right.

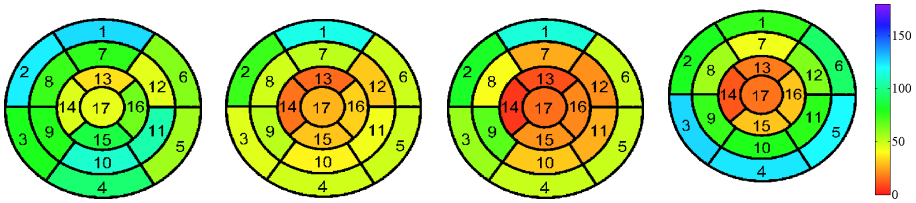

(a) 166 PMJs (b) 756 PMJs (c) 1,296 PMJs (d) EAM

Fig. 3. Mean endocardial LAT [ms] in the 17 AHA segments for the simulation using low, mid or high-density PN (from left to right), compared to the EAM (far right).

To analyse more closely the discrepancies observed in certain AHA segments, we present in Fig. 4 a box plot of the LAT in the EAM (top) and the simulation

(bottom). Segment medians and 25–75 percentiles are represented by the boxes, while outliers are denoted by red crosses (jitter added for enhanced readability). In segments 10–17 the existence of endocardial scarring divides the surface points in the simulation into an almost bimodal distribution – some points get activated early by the PMJs (denoted by points falling around the median) while others get activated late due to slow propagation in the deep scar region (the outliers). Comparing against the EAM we find that the median LAT in the EAM measurements is closer to the LAT of the simulation outliers, which may be either because the catheter measurements were not able to measure the PMJ-induced activation, or because the PMJs in the scar region were not activated. A similar situation exists in segments 3–5. Interestingly, in this case also the EAM measurements possess outliers but in the early activation region, which appears to indicate that at least some of the PMJ-induced activation was picked up by the catheter measurements. In the mid anterior segments without any scarring (7–9) the confidence intervals are roughly overlapping.

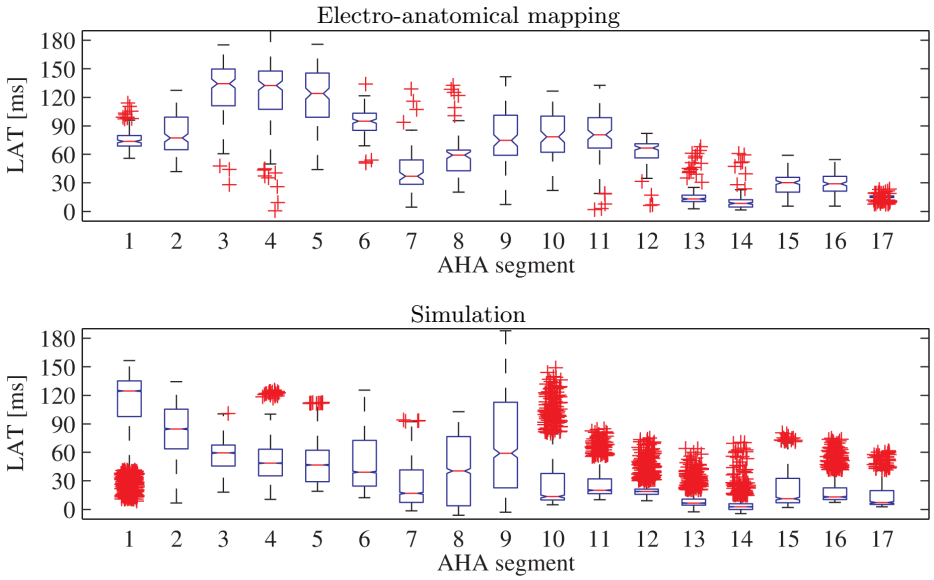

Fig. 4. Box plots of LAT for EAM (top) and simulation (bottom) grouped by AHA segment. Red crosses denote outliers that do not fall within the confidence intervals. The simulated LAT exhibits a strongly bimodal distribution in segments with scarring.

5 Discussion

We presented a pipeline for EP simulations on a patient-specific LV geometry. Even without personalising the PN or myofibre directions, reasonably good

agreement between simulated and experimental LAT was obtained, provided that the PMJs coverage was dense. Excitable myocytes had to be modelled in the myocardial scar to obtain correspondence between EAM and simulation. There may exist a viable sub-endocardial layer 3–5 cells deep (due to oxygen diffusion from the blood pool) that allows conduction to take place in the scar.

Our model has certain limitations. It does not account for transmural variations in the myocardial cells nor variations in the AP of the PN in ischemia; hence the validation centred mainly on the endocardial LAT. Further validation on multiple patient-specific instances is needed to study the transmural propagation and epicardial LAT should be performed, e.g. by comparing computed ECGs to those measured in vivo.

Acknowledgement *This research has been partially funded by the Industrial and Technological Development Center (CDTI) under the CENIT-cvREMOD program. The work of A.R. Porras and X. Albà was supported by the Spanish Government under FPU grant. A.F. Frangi was partially funded by the ICREA-Academia program. Clinical data used in this study was provided by A. Berruezo, D. Andreu, J. Fernández-Armenta, and M. Sitges from the Hospital Clinic of Barcelona.*

References

1. Andreu, D., Berruezo, A., Ortiz-Pérez, J., Silva, E., Mont, L., Borràs, R., de Caralt, T., Perea, R., Fernández-Armenta, J., Zeljko, H., et al.: Integration of 3D electroanatomic maps and magnetic resonance scar characterization into the navigation system to guide ventricular tachycardia ablation. Circ. Arrhythm. Electrophysiol. 4(5), 674–683 (2011)
2. Bogun, F., Good, E., Reich, S., Elmouchi, D., Igic, P., Tschopp, D., Dey, S., Wimmer, A., Jongnarangsin, K., Oral, H., et al.: Role of Purkinje fibers in post-infarction ventricular tachycardia. J. Am. Coll. Cardiol. 48(12), 2500–2507 (2006)
3. Bueno-Orovio, A., Cherry, E.M., Fenton, F.H.: Minimal model for human ventricular action potentials in tissue. J. Theor. Biol. 253(3), 544–560 (2008)
4. DiFrancesco, D., Noble, D.: A model of cardiac electrical activity incorporating ionic pumps and concentration changes. Phil. Trans. R. Soc. B 307(1133), 353–398 (1985)
5. Fernández-Armenta, J., Berruezo, A., Andreu, D., Camara, O., Silva, E., Serra, L., Barbarito, V., et al.: Three-dimensional architecture of scar and conducting channels based on high resolution CE-CMR insights for ventricular tachycardia ablation. Circ. Arrhythm. Electrophysiol. 6(3), 528–537 (2013)
6. Heidenreich, E., Rodríguez, J., Doblaré, M., Trénor, B., Ferrero, J.: Electrical propagation patterns in a 3D regionally ischemic human heart: A simulation study. In: IEEE Computers in Cardiology. pp. 665–668. IEEE (2009)
7. Lange, M., Lassila, T., Palamara, S., Vergara, C., Quarteroni, A., Frangi, A.: Efficient numerical schemes for computing cardiac electrical activation over realistic Purkinje networks: Method and verification. In: H. van Assen et al. (Eds.), Proc. 8th Int. Conf. Functional Imaging Model. Heart, FIMH 2015, Maastricht, The Netherlands, June 25–27, Springer LNCS 9126 pp. 430–438 (2015)

8. Lu, W., Wang, K., Zhang, H., Zuo, W.: Simulation of ECG under ischemic condition in human ventricular tissue. In: IEEE Computers in Cardiology. pp. 185–188. IEEE (2010)
9. Nattel, S., Maguy, A., Le Bouter, S., Yeh, Y.H.: Arrhythmogenic ion-channel remodeling in the heart: heart failure, myocardial infarction, and atrial fibrillation. Physiol. Rev. 87(2), 425–456 (2007)
10. Palamara, S., Vergara, C., Catanzariti, D., Faggiano, E., Pangrazzi, C., Centonze, M., Nobile, F., Maines, M., Quarteroni, A.: Computational generation of the Purkinje network driven by clinical measurements: the case of pathological propagations. Int. J. Numer. Methods Biomed. Engr. 30(12), 1558–1577 (2014)
11. Palamara, S., Vergara, C., Faggiano, E., Nobile, F.: An effective algorithm for the generation of patient-specific Purkinje networks in computational electrocardiology. J. Comp. Phys. 283, 495–517 (2015)
12. Porras, A., Piella, G., Berruezo, A., Fernández-Armenta, J., Frangi, A.: Pre-to intra-operative data fusion framework for multimodal characterization of myocardial scar tissue. IEEE J. Transl. Eng. Health Med. 2 (2015)
13. Porras, A., Piella, G., Berruezo, A., Hoogendoorn, C., Andreu, D., Fernandez-Armenta, J., Sitges, M., Frangi, A.: Interventional endocardial motion estimation from electroanatomical mapping data: Application to scar characterization. IEEE Trans. Biomed. Eng. 60(5), 1217–1224 (2013)
14. ten Tusscher, K.H., Panfilov, A.V.: Alternans and spiral breakup in a human ventricular tissue model. Am. J. Physiol. Heart C. 291(3), H1088–H1100 (2006)
15. Vergara, C., Palamara, S., Catanzariti, D., Nobile, F., Faggiano, E., Pangrazzi, C., Centonze, M., Maines, M., Quarteroni, A., Vergara, G.: Patient-specific generation of the Purkinje network driven by clinical measurements of a normal propagation. Med. Bio. Eng. Comput. 52(10), 813–826 (2014)
16. Vigmond, E., Clements, C.: Construction of a computer model to investigate sawtooth effects in the Purkinje system. IEEE Trans. Biomed. Eng. 54(3), 389–399 (2007)
17. Walker, N., Burton, F., Kettlewell, S., Smith, G., Cobbe, S.: Mapping of epicardial activation in a rabbit model of chronic myocardial infarction. J. Cardiovasc. Electrophysiol. 18(8), 862–868 (2007)